RomX, a novel prokaryotic regulator, links the response receiver domain of RomR with GTP-bound MglA for establishing *Myxococcus xanthus* polarity

Authors: Sukanya Chakraborty, and Pananghat Gayathri*

* Corresponding author: Pananghat Gayathri *

Indian Institute of Science Education and Research Pune, Dr Homi Bhabha Road, Pashan, Pune, India 411008.

Phone: +91-20-25908128

Email: gayathri@iiserpune.ac.in

Running title: RomX links the response receiver domain of RomR with MglA

Abbreviations: GEF: Gunanine nucleotide exchange factor; GAP: GTPase Activating Protein; *mant*: 2'/3'-O-(N-methyl anthraniloyl; GDP: guanosine diphosphate ; GTP: guanosine 5'-tri-phosphate; PDB: Protein Data Bank; RomR: Regulator of motility response regulator MglA: Mutual gliding protein A; MglB: Mutual gliding protein B; NADH: nicotinamide adenine dinucleotide; pLDDT: Predicted local distance difference test; ITC: Isothermal titration calorimetry; DALI: Distance Alignment matrix ; REC: Receiver domain; SAD: Single wavelength anomalous diffraction

Abstract

Cell polarity specification and reversals are distinctive features of motility of the soil bacterium *Myxococcus xanthus*. The bacterial small Ras-like GTPase, MglA, serves as a key player orchestrating these polarity oscillations. RomR, a response regulator, along with its partner RomX, has been identified as a guanine nucleotide exchange factor (GEF) for MglA, crucial for its polar recruitment. In this study, we determine the crystal structure of RomX, a protein of a hitherto unknown fold. RomX consists of a three-helix bundle, identified to be the same fold as the stalk domain of atlastin, a member of the dynamin family of GTPases. From our structure-based sequence analysis for proteins of similar fold, we observe the co-occurrence of the RomX fold with response receiver domains in several bacterial response regulators. We demonstrate that the binding between MglA and RomX is exclusively in the presence of GTP. Based on mutational analysis and affinity measurements, we conclude that the helix-1 of RomX mediates the interaction with MglA-GTP, while helix-3 of RomX interacts with the RomR N-terminal receiver (REC) domain. Absence of additional stimulation of RomX GEF activity in the presence of RomR-REC supports the mutually exclusive interface on RomX for RomR and MglA interaction. Collectively, our findings validate the positioning of RomX between MglA and RomR-REC, providing insights into the concerted action of the bipolarly localized RomR/RomX complex in driving MglA localization within polarized cells.

Keywords

RomX, Response regulator RomR, Prokaryotic small Ras-like GTPase MglA, GEF, *Myxococcus xanthus*, polarity reversal

Introduction

Rod-shaped *Myxococcus* cells possess a specified front-rear polarity that governs their directional movement[1–3]. The core of this oscillatory system consists of proteins exhibiting distinct subcellular localization patterns that determine the front-rear cell polarity[4,5]. Interestingly, *Myxococcus xanthus* undergoes frequent reversals in cell polarity, a phenomenon important in shaping its unique motility pattern which is also crucial for sustaining its life cycle[6–8]. This polarity reversal, associated with the redistribution of polarly localized proteins [9–11], prompts the cell to travel in the opposite direction. The frequency of cell polarity reversals is finely tuned by external chemosensory cues, which orchestrate the dynamic behavior of *Myxococcus xanthus* with respect to nutrient availability[12,13].

MglA is a prokaryotic small Ras-like GTPase, which acts as the major regulator driving *Myxococcus xanthus* polarity reversals[14–16]. Similar to other well-characterized eukaryotic small Ras-like GTPases, it switches between the active GTP-bound and inactive GDP-bound states[17–19]. This is associated with conformational change at regions near the nucleotide-binding pocket, also referred to as the Switch regions, that affects its localization and interaction with other proteins driving motility and reversals[17,20,21]. The active GTP bound state localizes to the leading cell pole and relocates to the opposite pole when the reversal switch is triggered. When the bound GTP is hydrolyzed, the protein in the GDP-bound state detaches from the pole and diffuses in the cytoplasm. In the active GTP bound state, it interacts with SgmX, an effector, and also plays a role in the correct polar localization of PilB and PilT ATPases, all of which are critical to S-motility[22–24]. It also interacts with AglZ in the GTP state, localizing to the focal adhesion complex-like gliding motors, and manifesting the cell movement[15,25–28].

Much like other small Ras-like GTPases, MglA has a very slow intrinsic GTP hydrolysis rate. This results in the requirement of a GTPase activating protein (GAP) which can assist GTP hydrolysis, thereby causing the GTPase to Switch from its “ON” GTP state to the “OFF” GDP

state. Further, MglA has a high affinity to GDP over GTP. This necessitates the requirement of a GEF that assists MglA in losing its affinity towards GDP, which consequently helps GTP association. Hence GEFs are essential to reactivate MglA from the “OFF” GDP bound state back to its “ON” GTP bound state.

Myxococcus xanthus MglA is regulated by various interactors that sense or modulate the bound nucleotide state, together driving the polarity reversal of this bacterium. MglB acts as the cognate GAP for MglA and accelerates the intrinsic slow GTP hydrolysis activity of MglA which in turn is further accelerated by a co-GAP, RomY[17–21,29]. MglB consists of a Roadblock domain, which has been shown to exert the GAP activity indirectly by orienting MglA active site residues in a conformation favoring GTP hydrolysis[21,30,31]. In addition, MglB consists of a C-terminal extension (MglB-Ct) which was shown to trigger the MglA GDP to GTP conformational switch[21,32]. Through an allosteric mechanism, MglB-Ct causes the strongly bound GDP to dissociate and consequently favors GTP binding, thereby acting as a candidate GEF for MglA. Simultaneous to the report of the GEF activity of MglB, a new regulator in the polarity reversal module, namely RomX was identified to act as a GEF for MglA together with its interacting partner RomR[33]. RomR is a multi-domain protein with an N-terminal response receiver domain (REC; 1-116 residues) and a C-terminal output domain (117- 420)[34]. The output domain consists of a long-disordered region followed by a conserved C-terminal tail (Ct region). Deletion of the REC domain impairs cellular reversals, suggesting that RomR relocalization is essential during reversals[35]. Both RomR and RomX were found to be essential for driving A-motility in *M. xanthus*[33,34]. The C-terminal output domain was critical for the correct polar localization of RomR[34,36].

RomX co-occurs with its partner, RomR across genomes[33]. In *M. xanthus* it was reported that the RomX polar localization is regulated by RomR. RomR interacts with RomX which further interacts with MglA to form a heteromeric complex and helps recruit MglA GTP to the leading pole[33]. RomX was shown to act as the active guanine nucleotide exchange factor (GEF) for MglA[33]. Together with RomR, it was observed to accelerate the GDP to GTP exchange on

MglA at a faster rate than RomX alone[33]. The main role of the GEF activity of RomR/RomX is hypothesized to be for recruiting MglA-GTP at or near the leading pole of the cell. In addition to its function at the leading pole, RomR-RomX also co-localizes with MglA GTP in the Agl/Glt focal adhesion complexes driving gliding motility[33]. However, in a polarized cell, RomR/RomX localizes in a bipolar asymmetric cluster, with a bigger cluster at the lagging pole, where MglA has to be excluded[33,34,37]. This leads us to a conundrum of how RomR-RomX could function to maintain the polar localization of MglA as observed in *Myxococcus* motility.

With a goal to obtain the mechanism of action of RomR-RomX, we report the crystal structure of RomX as a novel alpha-helical protein. Significantly, we observe RomX fold to be associated with the GTPase domain of the dynamin family of GTPases and also often to co-occur with response receiver domains of several bacterial response regulators. Our detailed biochemical characterization of the interacting interface of MglA and RomX highlights the residues important for complex formation exclusively in the GTP-bound conformation. A domain-wise dissection of RomR reveals that the receiver domain interacts with RomX. We demonstrate that RomX is sandwiched between MglA and RomR, and forms the preliminary anchor to selectively recruit MglA-GTP to the leading pole and the focal adhesion complexes. Our observations shed light on how an active mechanism of exclusion of MglA from the lagging pole involves a potential active recycling of GEF and GAP activities.

Results

RomX is monomeric and comprises a three-helix bundle

The hexahistidine-tagged RomX constructs were soluble and were purified with a high yield. (Supplementary Fig S1A). However, RomX, despite being an 11.4 kDa protein, eluted aberrantly (not according to the expected monomeric elution volume) at 13.3 ml in analytical size exclusion chromatography (SEC) (Supplementary Fig S1B). The secondary structure prediction of RomX reveals it to be a predominantly alpha-helical protein (Supplementary Fig S1C). To distinguish the oligomeric state of RomX, we performed SEC coupled with multi-angle light scattering (MALS) to confirm its oligomeric state. In SEC-MALS, the observed molar mass was 13.6 kDa (Fig 1A). Hence, we concluded that RomX was monomeric in solution. CD spectroscopy provided an alpha helical signature which confirmed that RomX was predominantly composed of alpha helices (Supplementary Fig S1D).

Since RomX was of unknown fold with no known structural homologs from sequence-based searches, we employed anomalous diffraction from selenomethionine-labeled protein to solve the crystal structure of RomX (Supplementary Fig. S1E). The single-wavelength anomalous scattering data was used to solve the structure to an overall resolution of 1.9 Å for the best crystal (Table 1). Upon solving the structure and consequent refinement, RomX was indeed found to be an alpha-helical protein (Fig. 1B), in which the helices constituted a three-helix bundle. There was one molecule in the asymmetric unit, and crystal-packing analysis further confirmed that it was monomeric.

RomX fold is similar to the stalk domain of the dynamin family and is associated with response receivers.

We used the experimentally determined structure of RomX to further identify proteins with similar fold (Supplementary Table S2). Interestingly, the stalk domain of atlastin in humans and Sey1p in yeasts were found to be most structurally similar to RomX (Fig 1C)[38–40] based

on output from DALI[41]. It is interesting to note that the occurrence of RomX fold in eukaryotes is associated with GTPases, since it has been shown earlier that RomX (along with RomR) functions as a regulator of the prokaryotic small Ras-like GTPase MglA. However, the connection between the stalk domain and the atlastin GTPase domain is away from the nucleotide-binding pocket, unlike interactions observed in typical GEFs, which sit near the nucleotide-binding pocket, competing out the bound GDP (Fig. 1C)[42–44].

Further, using the experimental structure of RomX, we performed a structure-based alignment using Foldseek[45]. Out of the hits from the AlphaFold database, many were models of uncharacterized bacterial proteins[46]. Out of the annotated models, the most common hits were of response regulatory proteins containing a receiver domain (Supplementary Table S2, Fig. 1D) and a RomX-fold domain in tandem. The other associated fold was of Zinc finger/ thioredoxin putative domain-containing bacterial proteins[47]. Significantly, the analysis reveals RomR/X-like complexes in many families of deltaproteobacteria, many of which are uncharacterized. This is an interesting observation in the context of *M. xanthus* RomX being associated with RomR which has an N-terminal response receiver (REC) domain.

RomX forms a complex with MglA only in the presence of GTP.

Next, we attempted to decipher the preferred nucleotide state for the interaction of MglA with RomX. Analytical SEC was carried out using MglA and RomX in the presence of GDP and GTP, respectively (Supplementary Fig. S2A, B). MglA and RomX eluted at 13.6 ml and 14 ml, respectively. These elution volumes of the peaks were too close to be resolved conclusively. Since there was no shift of the resultant peak of a complex of MglA and RomX towards a lower elution volume, we could not demonstrate any interaction between the two proteins in the presence of either nucleotide. Considering the plausible effects of dilution and aberrant elution volumes of the complex, we could not conclusively determine if RomX binds to MglA either in the presence of GTP or GDP.

To resolve this, we performed isothermal titration calorimetry (ITC) studies to quantify the interaction between MglA and RomX in the presence of nucleotides. There was no binding observed between MglA and RomX in the presence of excess GDP unlike what would be expected for a typical GEF (Supplementary Fig. S2C). Instead, when we performed titration in the presence of excess GTP (2 mM), we observed binding between MglA and RomX. We observed a K_d of 4.8 ± 0.5 μM and the stoichiometry of interaction N was 1.1 ± 0.1. This confirmed that RomX interacts with MglA in a 1:1 ratio in the presence of GTP. Based on the observed ΔH and ΔS values, the interaction is entropy-driven. The positive ΔH also rules out the possibility that the observed energy changes are the result of GTP hydrolysis, which is negligible in the absence of MglB.

Since we observed the binding of RomX with MglA in the presence of GTP, we estimated the effect of RomX on MglA GTP hydrolyzing activity to rule out the possibility of a GTPase activating protein (GAP) activity. There was no stimulation in the MglA GTP hydrolysis upon addition of RomX (Fig. 2B). The results were similar even when higher concentrations of RomX were used (1:4 MglA: RomX). MglA+MglB (1:2) was used as a positive control where the GAP stimulation of MglA was observed.

RomX helix-1 interacts with MglA-GTP, stimulating nucleotide exchange

We proceeded with measurement of the nucleotide exchange activity of the purified RomX as reported earlier[33]. Nucleotide exchange assays were performed where we monitored the *mant*-GMPPNP association (Fig. 2C). It was consistently observed that in the presence of RomX, MglA-GDP (purified MglA comes bound to GDP[21]) showed active nucleotide exchange and an increase in fluorescence was observed upon addition of MglA with RomX to *mant*-GMPPNP, compared to the addition of MglA alone. This demonstrated that RomX exerts a nucleotide exchange activity on MglA, in line with earlier reports. However, the interaction is probably not stable as we observe an intrinsic decrease in fluorescence intensity immediately after the association event. This also confirms that RomX indeed interacts with MglA,

consistent with the ITC measurements, however the interaction is not sufficient to exert a stabilization effect of the bound nucleotide. This is suggestive that the interaction might be transient given the comparatively high K_d.

Based on the interaction studies between MglA and RomX, we wanted to characterize the interface between MglA and RomX. Crystallization trials were unsuccessful till date possibly because of the transient nature of the complex. Hence, we used AlphaFold to generate a complex of MglA with RomX (Fig. 2D)[48]. The helix-1 from the N-terminal of RomX was seen to face toward the nucleotide-binding pocket of MglA. There are arginines (Arg-11, Arg-14) of RomX and glutamates (Glu-108, Glu-111,Glu-115) of MglA, which come in close proximity and could be holding the complex together. Moreover, Asp-19 faces towards the MglA nucleotide binding pocket near the Switch II, which could possibly be the residue driving the nucleotide specificity and exchange activity on MglA. Interestingly, all the 3 chosen interface residues, Arg-11, Arg-14, and Asp-19 of RomX are conserved (Fig. 2E), which indicates that these might be important for driving RomX function.

To confirm the RomX-MglA interface and the consequent mechanism of RomX GEF activity, we generated mutants of RomX. Firstly, we generated a double mutant where the Arg-11 and Arg-14 of RomX were mutated to alanines, intending to break the transient interaction with MglA ($RomX^{R11,R14A}$). We further mutated the Asp-19 of RomX, to alanine to abolish the GEF activity ($RomX^{D19A}$) (Fig. 2D). We purified the mutant proteins (Supplementary Fig. S2D) and confirmed using CD spectroscopy that they were well folded (Supplementary Fig. S2E). We then checked their respective GEF activity in the presence of MglA using nucleotide exchange assays (Fig. 2C). It was observed with our *mant*-GMPPNP exchange assays that, indeed, both the RomX mutants had their GEF activity completely abolished as compared to the wild-type RomX. We additionally performed ITC experiments for monitoring the binding of $RomX^{R11,R14A}$ with MglA in the presence of GTP (Fig. 2F). We observed no binding of this mutant to MglA-

GTP, confirming that these residues in RomX were indeed involved in MglA interaction, and that the GEF effect was correlated with the interaction.

RomX forms a high-affinity complex with RomR-REC domain.

Next, we characterized the interface between RomX and RomR, and consequently attempted to dissect the precise domain boundaries of RomR that interact with RomX (Fig. 3A). For the N-terminal REC domain, we chose till residues 125 and 141, respectively for the two different constructs tested, based on secondary structure prediction (Supplementary Fig. S3A). We cloned and expressed the REC domain constructs (RomR-REC^{125} and RomR-REC^{141}) of RomR (Fig. 3B) and recombinantly purified them (Supplementary Fig. 3B). A shorter construct of 1-116 residues was also attempted to be purified based on earlier reports[34]. However, it could not be successfully purified as the protein was unstable and probably aggregated during expression and purification steps. Next, the C-terminal domain, spanning residues 331-420 (based on secondary structure prediction), was cloned and successfully purified (Supplementary Fig. S3C). The C-terminal domain was found to be predominantly composed of alpha-helices as confirmed by CD spectroscopy (Supplementary Fig. S3D). According to secondary structure and Alphafold-based predictions, RomR-Ct helical domain is comprised of helices from residues 371-420, which is kinked in the center around the 396th residue (Supplementary Fig. S3E).

The purified constructs of RomR domains were subjected to analytical size exclusion chromatography with RomX. The RomR-REC^{125} in complex with RomX, resulted in a shift in the resultant peak to a higher volume (12.1 ml), as compared to individual peaks of RomR-REC^{125} (12.9 ml) and RomX (13.8 ml). This confirms the complex formation (Supplementary Fig. S4A). To determine the stoichiometry of the complex, we performed SEC-MALS to determine the molar mass corresponding to the peak of the complex (Fig. S3C). Using a Superdex 75 SEC column, there was a shift in the peak of the complex from 12.5 ml for RomR

REC^{141} and 14 ml for RomX to 11.5 ml. The observed molar mass was 24.6 kDa, corresponding to a 1:1 complex of RomR REC^{141} (14.5 kDa) and RomX (11.4 kDa).

Further, the binding affinity between RomR-REC^{125} and RomX complex was quantified using isothermal titration calorimetry (Fig. 3D). A similar titration experiment was performed with RomR REC^{141}, and the results were comparable. We obtained an average K_D of 1.14 ± 0.05 μM for RomR REC^{125} and RomX and 1.2 ± 0.5 μM for RomR REC^{141} and RomX (Fig. 3D). The stoichiometry of interaction was same for both RomR REC^{125} and RomR REC^{141}, 1.3 ± 0.2 and 1.2 ± 0.2, respectively, implying an interaction of one molecule of RomR REC domain with one molecule of RomX. The interaction was observed to be exothermic, and entropy-driven. Based on our comparable results between RomR-REC^{125} and RomR-REC^{141}, we can conclude that residues 1-125 consist of the minimal functional REC domain in RomR, capable of maintaining a stable RomX interaction.

Based on analytical SEC (Superdex 200), it was observed that the RomR-Ct helical domain does not interact with RomX. There was a clear separation of peaks observed at 12.3 ml for RomR-Ct and 17.6 ml for RomX (Fig. 3E). Further, using AlphaFold, we could not predict a reliable interface between RomR-Ct domain and RomX due to low pLDDT scores (Fig 3F)[38,49]. The SEC result indicates that the C-terminal helical domain alone of RomR does not form a stable complex with RomX.

Salt bridge interactions predominantly hold RomX and RomR-REC complex.

To characterize the interface between the RomR-REC domain and RomX, an AlphaFold model of the complex was predicted using one molecule each of RomX and RomR (1-125 residues) (Fig. 4A). The predicted RomX model superposed well with the experimentally obtained RomX structure with an RMSD of 0.8 Å. Analysis of the interface from the AlphaFold prediction of the complex, Glu-108 of RomR formed a salt bridge interaction with Arg-76 of RomX. Further, Val-17 of RomR and Leu-75 of RomX formed a hydrophobic core into which

Trp-87 of RomX stacks when in complex with RomR-REC. This tryptophan is exposed in solution in the crystal structure when RomX is monomeric. We checked the extent of conservation of these candidate interface residues both in RomR-REC and RomX. The Glu-108 in RomR is highly conserved (Fig. 4B), and so is the Trp-87 in RomX (Fig. 4C). The Arg-76 of RomX is often replaced with Lys, which highlights the importance of these basic residues at this position capable of forming the RomR-REC/RomX interface. It is important to note that according to the model, the candidate interface residues in RomX are part of helix-3.

Since Trp-87 was found to be the sole tryptophan residue in the RomRX complex showing a conformational transition across the monomeric RomX and RomRX complex, it could be used as a probe to monitor RomRX complex formation. The structure prediction was validated by monitoring the fluorescence of the single Trp-87 in RomX. Trp-87 is probably exposed in monomeric RomX and is buried in the RomRX complex interface. This would show up as a shift in the wavelength and intensity of the Trp emission maximum. Hence, RomX was titrated with an increasing concentration of RomR-REC^{125} (Fig. 4D). There was indeed a decrease in the Trp fluorescence intensity and a gradual blue shift in the emission maximum from 360 nm to near 330 nm (Fig. 4F, G). This indicated a reduction in the solvent-exposed environment of the Trp as the RomRX complex formed. This confirms that Trp-87 is one of the residues that inserts into the RomRX complex interface, a feature consistent with the AlphaFold prediction.

Based on our knowledge regarding the interface, we designed mutants of RomR and RomX, namely RomR-REC^{E108A} and RomX^{L75A,R76A} (L75, R76 both mutated to A). Since RomR-REC^{125} was found to be the minimal functional domain interacting with RomX, the E108A mutation was introduced in a RomR-REC^{125} background. Further, Trp fluorescence was measured using the interface mutants of RomR-REC and RomX. RomX^{L75A,R76A} mutant was titrated with increasing concentrations of RomR-REC^{E108A} (Fig. 3E). It was observed that there was no spectral shift compared to that of the wild-type RomR-REC^{125} and RomX (Fig. 3G). There was a slight reduction in the intensity of the emission maxima at higher concentrations of RomR-

REC (Fig. 3F). This was probably due to the crowding of RomR-REC molecules which masked the Trp-87 fluorescence signal minorly. This indicated that RomR-REC Glu-108, and RomX Arg-76 are important for complex formation, during which the Trp-87 stacks in the interface. To further validate this hypothesis, we performed ITC measurements to quantify the binding between RomR-REC^{E108A} and RomX^{L75A,R76A} (Fig. 3H). We did not observe binding between these mutant proteins further confirming that RomR-REC Glu-108, and RomX Arg-76 form a salt bridge interaction that holds the RomR-RomX complex together.

RomR-REC does not enhance the nucleotide exchange activity of RomX

We performed analytical SEC to dissect the interaction of the RomR-REC/RomX complex with MglA. No coelution was observed when the RomR-REC^{125}/RomX complex was injected with MglA. There was elution around 12.1 ml corresponding to the RomR-REC^{125}/RomX complex and at 13.1 ml to MglA, as verified by SDS PAGE to resolve the overlapping peaks (Supplementary Fig. S4A). This observation was consistent when the same experiment was performed in the presence of GDP and GTP, respectively. A similar result was even observed when the same set of runs were performed with RomR-REC^{141}.

Further, we investigated the interaction of RomR-Ct with MglA in analytical SEC (Supplementary Fig. S4B). There was a clear separation of peaks of RomR-Ct (12.8 ml) and MglA (around 16 ml), both in the presence or absence of nucleotides. This shows that there is no interaction of RomR-Ct with either RomX or MglA. All these observations indicate that there is probably no direct interaction between MglA and RomR-REC domain or the C-terminal tail.

Based on our information regarding the interface between MglA-RomX and RomX-RomR-REC, we conclude that RomX is probably sandwiched between MglA and the RomR-REC domain on either side. We used AlphaFold to confirm our model of MglA : RomX : RomR-REC

complex. The output AlphaFold model supports our idea that RomR-REC scaffolds RomX which further recognises and interacts with MglA-GTP (Fig. 5A).

We proceeded to check the role of all the RomR constructs in MglA GTPase activation (Fig. 5B) with and without RomX. It was observed that RomR-REC domain constructs and RomX alone or as a complex did not accelerate the rates of GTP hydrolysis by MglA. Expectedly, RomR-Ct also did not stimulate the GTPase activity of MglA. This indeed confirms that there is no stimulation of MglA-GTP hydrolysis by the RomR-RomX complex.

Since we observed the interaction of RomR-REC with RomX, we wanted to check if the presence of RomR-REC stimulates the GEF activity of RomX. We monitored the exchange of GDP bound to MglA in the presence of *mant*-GMPPNP (Fig. 5C). RomX induced a spontaneous nucleotide exchange on MglA, at similar rates with and without RomR-REC^{125}. RomR-REC^{125} alone did not stimulate nucleotide exchange by MglA. This showed that RomX alone drives nucleotide exchange on MglA without any additional contribution from the RomR REC. Expectedly, we did not observe any effect of RomR-Ct in the GEF stimulation of MglA (Fig 5D). Hence, in conclusion, RomX forms a complex with RomR-REC and MglA in the presence of GTP, confirming that RomX is sandwiched between its two interactors, with no direct interaction between MglA and RomR-REC. This is in line with previous hypothesis based on *in vivo* studies[33].

Discussion

We report the experimentally derived structure of RomX and identified the fold to be composed of a three-helix bundle. Through our structure-based fold search analyses, we identified the helical stalk domain of the dynamin family of GTPases as a structural homolog of RomX. The stalk domain in atlastin, especially, is shorter and closer to RomX owing to the presence of a three-helix bundle[38,49]. This domain is involved in the dimerization of the GTPase exclusively in the GTP-bound state to trigger hydrolysis driving membrane fusion[50]. The conformational changes in the stalk domain with respect to the GTPase domain in atlastin across nucleotide-bound states offer an interesting analogy in light of the specificity of RomX to MglA exclusively in the GTP-bound state. However, the atlastin stalk domain triggers nucleotide specificity for dimerization by altering the conformation of the switch regions through intramolecular interactions[33]. In contrast, RomX likely interacts near the nucleotide-binding pocket of MglA via helix-1, according to the Alphafold model, and further validated by our mutational studies in RomX. These residues also appear to be highly conserved, suggestive of a functional role for them. Confirmation of this interaction can be achieved through complementary mutations in MglA near the interface where RomX helix-1 interacts. However, mutating residues in MglA near the nucleotide-binding pocket often significantly destabilizes the protein, making binding studies such as ITC challenging to perform and interpret.

In line with the previous report, we observe that wild-type RomX stimulates nucleotide exchange activity on MglA. Additionally, the RomX helix-1 mutants abolish the exchange activity of RomX, further confirming the significance of this interface in nucleotide specificity and interaction with MglA. However, we do not detect any interaction between RomX and MglA-GDP, as would be expected for a typical GEF. This is again consistent with the previous report[33]. Based on these findings, we conclude that RomX predominantly interacts with and sequesters GTP-bound MglA, thereby promoting GDP to GTP exchange in MglA, which in turn drives the nucleotide exchange activity of RomX (Fig 6A).

Furthermore, our analyses also revealed that a RomX fold is often associated with a response receiver domain, which is prevalent in bacteria. Many of these proteins remain uncharacterized. This observation suggests that the interaction between the RomX-like fold and the receiver domain is conserved and likely integrated as a part of these individual response regulatory proteins. In the future, delving deeper into the mechanism of function of these multidomain response regulators and the role of the three-helix bundle RomX-like fold in these proteins will be of great interest.

We have determined that residues 1-125 constitute the minimal folded functional REC domain in RomR. Furthermore, we conclude that the REC domain of RomR interacts with RomX in 1:1 ratio. This explains why an exact co-localization of RomR with RomX in a bipolar asymmetric fashion is observed as per *in vivo* studies[33]. We hypothesize that the localization of RomX is largely a consequence of RomR's asymmetric bipolar localization. Specifically, the REC domain of RomR recruits RomX, in a 1:1 ratio to the cell poles, while the C-terminal output domain aids in recruiting other polar candidates[51]. Hence RomX localization simply mirrors the RomR localization pattern.

Our binding experiments demonstrate that helix-3 of RomX interacts with the RomR-REC domain, facilitated by salt-bridge interactions involving conserved residues in RomX helix-3 and RomR-REC. Given that RomX interacts with MglA via helix-1, positioned opposite to helix-3, it supports the idea that RomX is likely sandwiched between MglA and RomR-REC. Notably, we did not detect a direct interaction between MglA and RomR-REC. This observation is validated by the lack of further acceleration in the nucleotide exchange activity of RomX in the presence of RomR-REC. Conducting further *in vivo* experiments to assess the effects of interface mutants, as predicted in this study, will provide insights into the mechanism through which the RomR/X module contributes to maintaining MglA localization in a polarised cell.

In the cellular context, a pertinent question arises: why does a bigger RomR/X cluster persist at the lagging cell pole when its function as an MglA-GTP recruitment factor is primarily

exerted at the leading pole? It is to be noted that RomR serves as a polar scaffold not only for RomX but also for other polarly localized proteins such as MglC and MglB[51–54]. The substantial cluster of RomR at the lagging pole plays a crucial role in maintaining a refractory period, ensuring that a cell cannot be immediately triggered again after reversal[35]. We presume that there could also be a function of RomX localized at the lagging pole. MglA-GTP exhibits a higher affinity for MglB compared to RomX (approximately 5-fold), which may be further accentuated in the presence of RomY exclusively at the lagging cell pole[21,55]. In this scenario, RomX might facilitate the generation of localized pools of MglA-GTP at the lagging pole, facilitating its association with MglB/RomY due to its higher affinity (Fig. 6B). This GAP complex would actively trigger GTP hydrolysis, thereby excluding MglA-GDP from the lagging pole. The function of RomX as a MglA-GTP recruiter is primarily manifested at the leading pole and the Agl/Glt complexes, as previously hypothesized[33]. However, as this complex is inherently unstable, as per our observations, additional effectors such as SgmX, AglZ, or PilB may be required to stabilize the recruitment of MglA-GTP near the leading pole.

The structural characterization of RomX has helped us identify proteins containing domains of related fold among both eukaryotes and prokaryotes. It is interesting to observe the existence of RomX fold associated with the response receiver domain in the prokaryotes and with GTPases in higher eukaryotes, an observation with probable significance in the evolution of P-loop NTPases and cellular signaling mechanisms.

Materials and Methods

Cloning

Restriction-free cloning was performed for all the constructs. For the REC domain of RomR, residues 1-115 of the RomR gene was amplified from *romR- pETPhos* (obtained from Dr. Tam Mignot's lab) construct. It was cloned in *pHis17-Kan*^{R} vector with a C-terminal hexahistidine tag using respective primers (Supplementary Table S3). Further, a construct with N-terminal hexahistidine tag was cloned. Since the protein was impure, further 1-125 and 1-141 residues of the *romR* gene were cloned in the *pHis17-Kan*^{R} vector with a C-terminal hexahistidine tag. For the C-terminal, residues 331-420 *romR* gene were cloned in the *pHis17-Kan*^{R} vector with a C-terminal hexahistidine tag (insert amplified from *romR* gene synthesized from BioTechDesk). RomX gene (MXAN_3350) was amplified from *M. xanthus* genomic DNA (obtained from Dr. Tam Mignot's lab) and cloned into *pHis17-Amp*^{R} vector with both N and C-terminal hexahistidine tags. A similar strategy as mentioned above was also used to generate interface mutants of RomR and RomX. For the RomR-REC mutants, a RomR-REC^{125} background was used. MglA and MglB constructs used were as reported in Baranwal et al, 2019[21]. All clones were subjected to *DpnI* (New England Biolabs Inc.) digestion followed by transformation. Positive clones were selected on a suitable antibiotic (kanamycin and ampicillin, respectively) containing plates and checked by the consequent release of correct-sized fragments following double digestion with *NdeI* and *BamHI* (New England Biolabs Inc.). All the clones were confirmed by sequencing.

The list of constructs and the primers used in this study are tabulated in Supplementary Table S3.

Protein Expression

The constructs were transformed in BL21AI strains of *E. coli*. The cultures were grown in respective antibiotic-containing media (1X LB with 0.1 mg/ml ampicillin or 0.05 mg/ml kanamycin) and were kept in shaking conditions at 37°C. The cultures were induced with 0.2% L-Arabinose once it reached the exponential phase of growth (between 0.6-0.8 OD). The cultures were incubated overnight at 18ºC. The samples were subjected to 15% SDS-PAGE to observe the overexpressed protein band of interest. Further, the selenomethionine-labeled protein was expressed in minimal media supplemented with selenomethionine using feedback inhibition method and was consequently purified.

Protein purification

Purifications of MglA and MglB were performed as described in reference [21]

His-tagged affinity purification: As a first step, the harvested cells were resuspended in the lysis buffer (50 mM Tris pH 8.0, 200 mM NaCl, and 10% glycerol) at 4°C. Consequently, the samples were centrifuged at 39,000 g for 45 minutes. The lysate was loaded on a 5 ml HisTrap HP (GE Healthcare) column. The loading buffer was 200 mM NaCl, 50 mM Tris pH 8.0, and the elution buffer was 200 mM NaCl, 50 mM Tris pH 8.0, and 500 mM Imidazole. Protein was eluted using a stepwise gradient of 2%, 5%, 10%, 20%, 50%, and 100% elution buffer.

Size Exclusion chromatography: For the RomX constructs, this step was performed after Ni-NTA affinity chromatography. The column was equilibrated with 50 mM NaCl, 50 mM Tris pH 8.0 (A50) buffer. For analytical runs, approximately 2-3 mg/ml, 200 µL of protein was injected into the Superdex 75 or Superdex200 size exclusion column (GE Healthcare) (volume less than 900 µL for preparative runs). UV absorbance at 280 nm was observed to monitor the elution of the protein. The respective fractions were pooled, concentrated, and stored.

Anion Exchange (MonoQ): For RomR constructs, to improve the purity, this step was performed after Ni-NTA affinity chromatography. Hence, it was injected in MonoQ 4.6/100 PE (GE Healthcare). Buffers used for binding and elution were Buffer A (50 mM Tris [pH 8.0], 50

mM NaCl) and Buffer B (50 mM Tris [pH 8.0], 1 M NaCl), respectively. A linear gradient of Buffer A ranging from 0% to 50% Buffer B over 20 column volumes was injected, and the fractions containing the protein were pooled and concentrated.

Crystallization and structure solution

To determine the experimental structure of RomX, constructs with both C-terminal and N-terminal hexahistidine tags, were subjected to crystallization screens. Nearly 500 conditions of commercially available screens (Molecular dimensions, Hampton Research, Jena Bioscience, Rigaku) were screened using Mosquito crystallization robotic system, with drop sizes of 100 nl of protein at a concentration of 15 mg/ml and 100 nl of crystallization condition, in 96-well sitting drop plates (MRC plate, SWISS-SCI) There were multiple hits obtained for C-His-RomX but none for N-His-RomX. This shows that the position of the hexahistidine tag might affect crystal packing and hence, consequently, affect the possibility of better crystallization of the protein. After multiple rounds of optimization, the condition that gave the best reproducible crystals was with 25% PEG MME 550, 5 mM MgCl2, and 50 mM HEPES Na, pH 7 using the hanging drop method. The crystals were long, needle-shaped. Since RomX was found to be a novel protein with no known structural homologs, we had to employ anomalous diffraction techniques using selenomethionine-labeled protein to determine the phase of the diffraction data to solve the crystal structure (Supplementary Fig. 1E). The protein was crystallized in the same aforementioned condition. The anomalous scattering data was obtained and an overall resolution of 1.9 Å was obtained for the best crystal.

Diffraction data was collected from Diamond Light Source, UK. RomX anomalous data were collected at a wavelength of 0.9793 with f'=8.03 and f''=3.85. Data was reduced and scaled using iMOSFLM and AIMLESS, respectively, using the CCP4i2 package. Autosol and Autobuild wizards of PHENIX were used to build the model which was finally refined to satisfactory R_{work} and R_{free} values using iterative refinement cycles using Coot. The refinement statistics for each structure were tabulated to validate the quality of the refined data.

SEC-MALS

Size exclusion chromatography coupled with Multi-angle light scattering (SEC-MALS) experiments enabled the accurate molar mass estimation. The Superdex 75/200 Increase 10/300 GL column was used for SEC, which was connected to an Agilent HPLC unit with an 18-angle light scattering detector (Wyatt Dawn HELIOS II) and a refractive index detector (Wyatt Optilab T-rEX). The experiments were performed at room temperature. The column was equilibrated with A50 (50 mM NaCl, 50 mM Tris pH 8.0) buffer at 0.4 ml/min. BSA at 2 mg/ml was used to calibrate the system. The purified protein/complexes (approximately 5 mg/ml, 110 µL) were loaded to estimate the molecular weight of the eluted peaks. The Zimm model implemented in ASTRA software was used for the curve fitting and estimation of molecular weights. GraphPad Prism was used to average molar mass from fitted plots.

Isothermal Titration calorimetry

The proteins (MglA, RomR-REC and RomX) used for interaction studies were dialyzed into 20 mM phosphate buffer (K2HPO4+KH2PO4), pH 8, overnight and the exact concentrations were estimated using Bradford assay. For MglA and RomX runs, 2 mM $MgCl_2$ and 5 mM of nucleotide (GDP/GTP) were additionally supplemented in the reaction. ITC measurements were carried out by titrating 300 µM of RomX (N-terminal hexahistidine tagged construct) into 20 µM of RomR-REC in the sample cell using the MicroCal PEAQ-ITC, using a stirring speed of 750 rpm. 19 injections, 2 µl each were made. Similarly for MglA-RomX runs, measurements were carried out by titrating 1 mM of RomX (N-terminal hexahistidine tagged construct) into 50 µM of MglA in the sample cell using a stirring speed of 750 rpm. 19 injections, 1 µl each were made. Data for each experiment was modeled using a one-site binding model provided in the MicroCal PEAQ- ITC analysis software with fitted offset control. Error in K_d, N, ΔG, ΔH and -TΔS was calculated as the standard error of the mean using multiple replicates.

Tryptophan Fluorescence Assay

The experiment was performed in 20 mM phosphate buffer (K_2HPO_4+KH_2PO_4), pH=8. The sample volume was 200 µl in a quartz cuvette (10 × 2 mm path length) and excitation and emission slit widths of 2 nm. The excitation spectra were recorded between 200-300 nm. The emission spectra were recorded at the excitation wavelength of 287 nm and the emission spectra were recorded between 300-450 nm. 10 µM RomX was added to the buffer and the spectra were recorded. Further, it was titrated with 1-20 µM RomR in steps of 1 µM each. The emission maxima (λ_{max}) and the corresponding fluorescence intensity (in CPS, counts per second) were recorded and plotted against the concentration of RomR to estimate binding.

CD Spectroscopy

Far-UV CD spectra were collected using a Jasco J-815 spectropolarimeter with a protein concentration of 10 µM in a 1 mm cuvette, using a scan speed of 50 nm/min, a digital integration time of 2 s, and a bandwidth of 1 nm. Spectra was collected between 200 to 250 nm under permissive high-tension voltage. Each spectrum was averaged for over 30 scans. Spectra were deconvoluted and analyzed using BeStSel[56].

NADH-coupled GTP hydrolysis assay

NADH-coupled enzymatic assay [57], similar to the protocol used in reference [21]was used to measure GTP hydrolysis activity. A master mix was prepared in A50 buffer (50 mM NaCl, Tris pH 8.0) containing 600 µM NADH, 1 mM phosphoenol pyruvate, 5 mM $MgCl_2$, 1 mM GTP and pyruvate kinase and lactate dehydrogenase enzyme mix (~25 U/ml). All components were mixed to a 200 µl reaction volume and added to a Corning 96 well flat bottom plate. The reactions were initiated by adding purified protein complexes in respective ratios to a final concentration of 10 µM MglA. A decrease in NADH absorbance was measured at 340 nm using a Varioskan Flash (4.00.53) multimode plate reader. The absorbance was measured every 20 s for 7200 s. The initial time point and absorbance of buffer components were subtracted from all readings. NADH absorbance was converted to GDP produced using a

slope obtained from a standard curve containing known concentrations of NADH. GraphPad Prism was used for data analysis and plotting the k_{obs} values.

Nucleotide exchange assay

The kinetic measurements were performed on Fluoromax-4 (Horiba), where the intensity of fluorescence emission by *mant*-labeled GDP/GMPPNP (Jena Bioscience, Germany) at 440 nm was monitored after the excitation at 360 nm (protocol similar to the one used in[21]). The sample volume was 200 µl in a quartz cuvette (10 × 2 mm path length) and excitation and emission slit widths of 2 nm. *mant*-GDP/GMPPNP (final concentration 800 nM) was present in buffer A50 (50 mM Tris pH 8.0, 50 mM NaCl, 5 mM $MgCl_2$). The protein mix, i.e., a final concentration of 3 µM of the respective protein complexes, was added in the cuvette at 400 seconds after stabilization of the signal from only *mant*-nucleotide. Consequently, the fluorescence was recorded for 1,400 seconds, and the increase in intensity reflected the nucleotide-binding kinetics. At 1,800 seconds, the *mant*-labeled nucleotide was competed out with an excess of unlabeled GDP/GTP (final concentration 500 µM), resulting in the release of *mant*-labeled nucleotide from the protein which manifested as a decrease of fluorescence intensity. For plotting the relative intensities from the measurements, each value was divided by the average of the first 200 readings (400 seconds). These accumulations and decay reactions were fitted to exponential binding equations as given below in GraphPad Prism to estimate the k_{on} and k_{off} values.

$P + N_1 \rightarrow PN_1 + N_2 \rightarrow PN_2 + N_1$, where P represents protein, N_1 is the labeled nucleotide, N_2 is the unlabeled nucleotide, and PN denotes the protein-nucleotide complex.

For estimation of k_{on}, $PN_t = PN_{max} (1 - e^{-kt})$.

For estimation of k_{off}, $PN_t = PN_{max} - PN_{min} (e^{-kt}) + PN_{min}$

Here, PN_t represents the amount of the complex at time t, PN_{max} is the maximum amount of the complex upon association, and PN_{min} is the minimum amount of the complex after dissociation.

Bioinformatics

The structure of RomX was given as input to the DALI server to perform a structure-based search against the Protein Data Bank database[41]. It returned several hits for proteins with one or more chains in the same fold as RomX (coiled-coil helices) from within the PDB. The top 50 structures in the DALI output were analyzed and based on the RMSD values obtained, a total of 19 structures were shortlisted for further analysis (Supplementary Table S1).

For the Foldseek search, the structure of RomX was given as input to search against AFDB Proteome, AFDB SwissProt, AFDB50, CATH50 MGNIFY_ESM30, and PDB100 databases[45,58]. Most of the hits were obtained from the AFDB50 database. Out of 471 hits, 52 contained response regulatory proteins from bacteria, whereas the majority were uncharacterized proteins. The list of hits containing response regulatory domains is tabulated in Supplementary Table S2.

For sequence alignments of RomX and RomR-REC, NCBI BLASTp was used. Myxococcales (taxid:29) were excluded from the search. The hits were sorted according to the decreasing E-value. Alignments were generated using the top 500 hits and the conservation was represented using WEBLOGO.

Acknowledgments

The study was funded by the CEFIPRA Collaborative Research Grant (CSRP 5803-1) and supported by common instrumentation facilities at IISER Pune. SC acknowledges IISER Pune, Infosys Foundation, Biochemical Society, UK, DBT (DBT/CTEP/02/20220753076) for fellowships. Synchrotron facility at Diamond Light Source, UK, and the macromolecular crystallography facility at the National Centre for Cell Science, Pune, are acknowledged for data collection and crystal screening, respectively. Kushan Lahiri and Ranjana Nataraj are acknowledged for initiating the RomX fold search analyses and RomR-X docking studies. Dr Radha Chauhan and Jyotsana Singh from the National Centre for Cell Science, Pune, are acknowledged for their assistance in using the SEC-MALS facility. Suman Pal, Preeti Kumari and Prof. Jayant Udgaonkar are acknowledged for their assistance with CD spectroscopy experiments and access to the facility. Prof. Tam Mignot from CNRS, Marseille is acknowledged for providing the RomR plasmid from which the REC domain constructs were cloned.

Author Contributions

SC: Designed and performed all the experiments and wrote the manuscript

PG: Conceptualized the study, supervised the experiments and analyses, and reviewed and edited the manuscript

CrediT authorship contribution statement:

SC: Methodology; Investigation; writing - original draft

PG: Conceptualization; Methodology; Funding acquisition; Project administration; Supervision; Writing - review and editing

Declaration of competing interest

The authors declare no conflict of interest.

References

1. Kaiser D, Warrick H (2014) Transmission of a signal that synchronizes cell movements in swarms of Myxococcus xanthus. Proceedings of the National Academy of Sciences [Internet] 111:13105–13110. Available from: http://www.pnas.org/cgi/doi/10.1073/pnas.1411925111

2. Spormann AM, Kaiser D (1999) Gliding mutants of Myxococcus xanthus with high reversal frequencies and small displacements. J Bacteriol 181:2593–2601.

3. Kaiser D, Robinson M, Kroos L (2010) Myxobacteria, polarity, and multicellular morphogenesis. Cold Spring Harb Perspect Biol 2:1–26.

4. Herrou J, Mignot T Dynamic polarity control by a tunable protein oscillator in bacteria. Curr Opin Cell Biol [Internet] 62. Available from: https://hal-amu.archives-ouvertes.fr/hal-02459706

5. Igoshin O a, Goldbeter A, Kaiser D, Oster G (2004) A biochemical oscillator explains several aspects of *Myxococcus xanthus* behavior during development. Proc Natl Acad Sci U S A 101:15760–15765.

6. Mauriello EM, Zusman DR (2007) Polarity of motility systems in Myxococcus xanthus. Curr Opin Microbiol 10:624–629.

7. Zusman DR, Scott AE, Yang Z, Kirby JR (2007) Chemosensory pathways, motility and development in Myxococcus xanthus. Nat Rev Microbiol 5:862–872.

8. Keilberg D (2013) Regulation of motility and polarity in Myxococcus xanthus.

9. Zhang Y, Ducret A, Shaevitz J, Mignot T (2012) From individual cell motility to collective behaviors: Insights from a prokaryote, Myxococcus xanthus. FEMS Microbiol Rev 36:149–164.

10. Mignot T, Merlie JP, Zusman DR (2005) Regulated pole-to-pole oscillations of a bacterial gliding motility protein. Science (1979) 310:855–857.

11. Mauriello EMF, Mignot T, Yang Z, Zusman DR (2010) Gliding Motility Revisited: How Do the Myxobacteria Move without Flagella? Microbiology and Molecular Biology Reviews 74:229–249.

12. Kaimer C, Berleman JE, Zusman DR (2012) Chemosensory signaling controls motility and subcellular polarity in Myxococcus xanthus. Curr Opin Microbiol 15:751–757.

13. Eckhert E, Rangamani P, Davis AE, Oster G, Berleman JE (2015) Dual biochemical oscillators may control cellular reversals in myxococcus xanthus. Biophys J [Internet] 107:2700–2711. Available from: http://dx.doi.org/10.1016/j.bpj.2014.09.046

14. Hartzellt P, Kaiser D Function of MglA, a 22-Kilodalton Protein Essential for Gliding in Myxococcus xanthus. 1991.

15. Mauriello EMF, Mouhamar F, Nan B, Ducret A, Dai D, Zusman DR, Mignot T (2010) Bacterial motility complexes require the actin-like protein, MreB and the Ras homologue, MglA. EMBO Journal 29:315–326.

16. Treuner-Lange A, Macia E, Guzzo M, Hot E, Faure LM, Jakobczak B, Espinosa L, Alcor D, Ducret A, Keilberg D, et al. (2015) The small G-protein MglA connects to the MreB actin cytoskeleton at bacterial focal adhesions. Journal of Cell Biology 210:243–256.

17. Miertzschke M, Koerner C, Vetter IR, Keilberg D, Hot E, Leonardy S, Søgaard-Andersen L, Wittinghofer A (2011) Structural analysis of the Ras-like G protein MglA and its cognate GAP MglB and implications for bacterial polarity. EMBO Journal 30:4185–4197.

18. Zhang Y, Franco M, Ducret A, Mignot T (2010) A Bacterial Ras-Like Small GTP-Binding Protein and Its Cognate GAP Establish a Dynamic Spatial Polarity Axis to Control Directed Motility. PLoS Biol 8:e1000430.

19. Leonardy S, Miertzschke M, Bulyha I, Sperling E, Wittinghofer A, Søgaard-Andersen L (2010) Regulation of dynamic polarity switching in bacteria by a Ras-like G-protein and its cognate GAP. EMBO Journal 29:2276–2289.

20. Galicia C, Lhospice S, Varela PF, Trapani S, Zhang W, Navaza J, Herrou J, Mignot T, Cherfils J (2019) MglA functions as a three-state GTPase to control movement reversals of Myxococcus xanthus. Nat Commun 10:5300.

21. Baranwal J, Lhospice S, Kanade M, Chakraborty S, Gade PR, Harne S, Herrou J, Mignot T, Gayathri P (2019) Allosteric regulation of a prokaryotic small Ras-like GTPase contributes to cell polarity oscillations in bacterial motility. PLoS Biol 17:e3000459.

22. Mercier R, Bautista S, Delannoy M, Gibert M, Guiseppi A, Herrou J, Mauriello EMF, Mignot T The polar Ras-like GTPase MglA activates type IV pilus via SgmX to enable twitching motility in Myxococcus xanthus. Available from: www.pnas.org/cgi/doi/10.1073/pnas.2002783117

23. Bautista S, Schmidt V, Guiseppi A, Mauriello EMF, Attia B, Elantak L, Mignot T, Mercier R (2023) FrzS acts as a polar beacon to recruit SgmX, a central activator of type IV pili during Myxococcus xanthus motility. EMBO J 42.

24. Potapova A, Carreira LAM, Søgaard-Andersen L (2020) The small GTPase MglA together with the TPR domain protein SgmX stimulates type IV pili formation in *M. xanthus*. Proceedings of the National Academy of Sciences 117:23859–23868.

25. Nan B, Zusman DR (2011) Uncovering the mystery of gliding motility in the myxobacteria. Annu Rev Genet 45:21–39.

26. Nan B, Mauriello EMF, Sun IH, Wong A, Zusman DR (2010) A multi-protein complex from Myxococcus xanthus required for bacterial gliding motility. Mol Microbiol 76:1539–1554.

27. Nan B, Bandaria JN, Moghtaderi A, Sun IH, Yildiz A, Zusman DR (2013) Flagella stator homologs function as motors for myxobacterial gliding motility by moving in helical trajectories. Proc Natl Acad Sci U S A 110.

28. Nan B, Bandaria JN, Guo KY, Fan X, Moghtaderi A, Yildiz A, Zusman DR (2015) The polarity of myxobacterial gliding is regulated by direct interactions between the gliding motors and the Ras homolog MglA. Proc Natl Acad Sci U S A [Internet] 112:E186-93. Available from: http://www.pnas.org/content/112/2/E186.short

29. Szadkowski D, Carreira LAM, Søgaard-Andersen L (2022) A bipartite, low-affinity roadblock domain-containing GAP complex regulates bacterial front-rear polarity. PLoS Genet 18:e1010384.

30. Kanade M, Chakraborty S, Shelke SS, Gayathri P (2020) A Distinct Motif in a Prokaryotic Small Ras-Like GTPase Highlights Unifying Features of Walker B Motifs in P-Loop NTPases. J Mol Biol 432:5544–5564.

31. Galicia C, Lhospice S, Varela PF, Trapani S, Zhang W, Navaza J, Herrou J, Mignot T, Cherfils J (2019) MglA functions as a three-state GTPase to control movement reversals of Myxococcus xanthus. Nat Commun 10.

32. Chakraborty Sukanya, Kanade Manil, Gayathri Pananghat (2023) Mechanism of GTPase activation of a prokaryotic small Ras-like GTPase MglA by an asymmetrically interacting MglB dimer. Biorxiv.

33. Szadkowski D, Harms A, Carreira LAM, Wigbers M, Potapova A, Wuichet K, Keilberg D, Gerland U, Søgaard-Andersen L (2019) Spatial control of the GTPase MglA by localized RomR–RomX GEF and MglB GAP activities enables Myxococcus xanthus motility. Nat Microbiol 4:1344–1355.

34. Leonardy S, Freymark G, Hebener S, Ellehauge E, Søgaard-Andersen L (2007) Coupling of protein localization and cell movements by a dynamically localized response regulator in Myxococcus xanthus. EMBO Journal 26:4433–4444.

35. Guzzo M, Murray SM, Martineau E, Lhospice S, Baronian G, My L, Zhang Y, Espinosa L, Vincentelli R, Bratton BP, et al. (2018) A gated relaxation oscillator mediated by FrzX controls morphogenetic movements in Myxococcus xanthus. Nat Microbiol 3:948–959.

36. Zhang Y, Guzzo M, Ducret A, Li Y-Z, Mignot T (2012) A Dynamic Response Regulator Protein Modulates G-Protein–Dependent Polarity in the Bacterium Myxococcus xanthus. PLoS Genet [Internet] 8:e1002872. Available from: http://dx.plos.org/10.1371/journal.pgen.1002872

37. Keilberg D, Wuichet K, Drescher F, Søgaard-Andersen L (2012) A Response Regulator Interfaces between the Frz Chemosensory System and the MglA/MglB GTPase/GAP Module to Regulate Polarity in Myxococcus xanthus. PLoS Genet 8:e1002951.

38. O'Donnell JP, Byrnes LJ, Cooley RB, Sondermann H (2018) A hereditary spastic paraplegia-associated atlastin variant exhibits defective allosteric coupling in the catalytic core. Journal of Biological Chemistry 293:687–700.

39. Bian X, Klemm RW, Liu TY, Zhang M, Sun S, Sui X, Liu X, Rapoport TA, Hu J (2011) Structures of the atlastin GTPase provide insight into homotypic fusion of endoplasmic reticulum membranes. Proceedings of the National Academy of Sciences 108:3976–3981.

40. Yan L, Sun S, Wang W, Shi J, Hu X, Wang S, Su D, Rao Z, Hu J, Lou Z (2015) Structures of the yeast dynamin-like GTPase Sey1p provide insight into homotypic ER fusion. Journal of Cell Biology 210:961–972.

41. Holm L Using Dali for Protein Structure Comparison. In: ; 2020. pp. 29–42.

42. Cherfils J, Zeghouf M (2013) Regulation of Small GTPases by GEFs, GAPs, and GDIs. Physiol Rev [Internet] 93:269–309. Available from: www.prv.org

43. Toma-Fukai, Shimizu (2019) Structural Insights into the Regulation Mechanism of Small GTPases by GEFs. Molecules 24:3308.

44. Bos JL, Rehmann H, Wittinghofer A (2007) GEFs and GAPs: Critical Elements in the Control of Small G Proteins. Cell 129:865–877.

45. Hutson M (2023) Foldseek gives AlphaFold protein database a rapid search tool. Nature.

46. David A, Islam S, Tankhilevich E, Sternberg MJE (2022) The AlphaFold Database of Protein Structures: A Biologist's Guide. J Mol Biol 434:167336.

47. Xu Y, Kersten RD, Nam S-J, Lu L, Al-Suwailem AM, Zheng H, Fenical W, Dorrestein PC, Moore BS, Qian P-Y (2012) Bacterial Biosynthesis and Maturation of the Didemnin Anti-cancer Agents. J Am Chem Soc 134:8625–8632.

48. Jumper J, Evans R, Pritzel A, Green T, Figurnov M, Ronneberger O, Tunyasuvunakool K, Bates R, Žídek A, Potapenko A, et al. (2021) Highly accurate protein structure prediction with AlphaFold. Nature 596:583–589.

49. Hu X, Wu F, Sun S, Yu W, Hu J (2015) Human atlastin GTPases mediate differentiated fusion of endoplasmic reticulum membranes. Protein Cell 6:307–311.

50. Byrnes LJ, Singh A, Szeto K, Benvin NM, O'Donnell JP, Zipfel WR, Sondermann H (2013) Structural basis for conformational switching and GTP loading of the large G protein atlastin. EMBO J 32:369–384.

51. Carreira LAM, Szadkowski D, Lometto S, Hochberg GeorgKA, Søgaard-Andersen L (2023) Molecular basis and design principles of switchable front-rear polarity and directional migration in Myxococcus xanthus. Nat Commun 14:4056.

52. Carreira LAM, Szadkowski D, Müller F, Søgaard-Andersen L (2022) Spatiotemporal regulation of switching front–rear cell polarity. Curr Opin Cell Biol 76.

53. Kapoor S, Kodesia A, Kalidas N, Ashish, Thakur KG (2021) Structural characterization of Myxococcus xanthus MglC, a component of the polarity control system, and its interactions with its paralog MglB. Journal of Biological Chemistry 296:100308.

54. McLoon AL, Wuichet K, Häsler M, Keilberg D, Szadkowski D, Søgaard-Andersen L (2016) MglC, a paralog of Myxococcus xanthus GTPase-activating protein MglB, plays a divergent role in motility regulation. J Bacteriol 198:510–520.

55. Szadkowski D, Carreira LAM, Søgaard-Andersen L (2022) A bipartite, low-affinity roadblock domain-containing GAP complex regulates bacterial front-rear polarity. PLoS Genet 18.

56. Micsonai A, Wien F, Bulyáki É, Kun J, Moussong É, Lee YH, Goto Y, Réfrégiers M, Kardos J (2018) BeStSel: A web server for accurate protein secondary structure prediction and fold recognition from the circular dichroism spectra. Nucleic Acids Res 46:W315–W322.

57. Kiianitsa K, Solinger JA, Heyer WD (2003) NADH-coupled microplate photometric assay for kinetic studies of ATP-hydrolyzing enzymes with low and high specific activities. Anal Biochem 321:266–271.

58. van Kempen M, Kim SS, Tumescheit C, Mirdita M, Lee J, Gilchrist CLM, Söding J, Steinegger M (2024) Fast and accurate protein structure search with Foldseek. Nat Biotechnol 42:243–246.

Tables

Table 1. Data Collection and refinement statistics of RomX (Values in parentheses denote the last resolution shell)

Collected at	Diamond Light Source
Wavelength	0.9793
Data Collection Statistics	
Space group	$P2_12_12_1$
a,b,c (Å)	33.3, 56.1, 68.6
α, β, γ (°)	90, 90, 90
Resolution (Å)	1.9
No. of unique reflections	266856 (8682)
R_{merge} (%)	11.5 (117.3)
R_{pim} (%)	3.2 (41.1)
CC_{half}	0.999 (0.699)
Mean I/sigmaI	19.1 (2.0)
Completeness (per cent)	99.1 (86.6)
Refinement Statistics	
Resolution (angstrom)	29.955-1.88
No. of reflections	19678
R_{work}/R_{free} (%)	18.91/22.16
Average B factor ($Å^2$)	33.71
Wilson B factor ($Å^2$)	27.67
RMS deviation	
Bond lengths (Å)	0.003
Bond angles (°)	0.480
Ramachandran Map	
Favoured (%)	97.8
Allowed (%)	2.2
Outliers (%)	0

Table 2. Stoichiometry, affinity, and thermodynamic parameters corresponding to the ITC experiments.

	K_d (μM)	*N*	*ΔH (kcal/mol)*	*ΔG (kcal/mol)*	*-TΔS (kcal/mol)*
MglA+RomX+GTP	4.5 ± 0.5	1.1 ± 0.1	2.7 ± 0.3	-7.32 ± 0.07	9.9 ± 0.3
RomR-REC^{125}+RomX	1.4 ± 0.3	1.3 ± 0.2	-1.6 ± 0.3	-8.1 ± 0.02	-5.31 ± 0.3
RomR-REC^{141}+RomX	1.15 ± 0.05	1.3 ± 0.2	2.7 ± 0.3	-8.0 ± 0.1	-6.5 ± 0.3

Figure Legends

Figure 1. RomX is monomeric, alpha-helical, and consists of a fold associated with GTPases and response regulators.

A: Superdex 200 SEC MALS run for RomX. The protein elutes at 17.7 ml and the observed molar mass is 13.6 kDa (±1.964%). The molar mass is represented in dark green and the dRI is represented in light green.

B: Crystal structure of C-His RomX solved with anomalous diffraction. There was one molecule in the asymmetric unit. The N and C termini of the protein are labelled.

C: Superposition of RomX structure on the stalk domain of Atlastin (4IDN), a member of the dynamin family GTPase.

D. Superposition of RomX structure with a response regulatory domain-containing protein from *Delsulfuromonas sp.* The receiver domain and the ZnF/thioredoxin domains are shown in green and coral respectively. The experimental structure of RomX (in cyan) is superposed on the helical domain (in dark purple)

Figure 2. RomX preferentially interacts with MglA-GTP near the nucleotide-binding pocket, stimulating exchange.

A: ITC thermogram of a representative binding assay showing the titration of RomX with MglA in the presence of GTP and magnesium. The left panel shows the raw data of endothermic heat pulses with time. The middle panel shows the corresponding differential binding curve fitted to a single-site binding model. The right panel shows the signature plot detailing the ΔG, ΔH, and -TΔS values corresponding to the same reaction (mean and standard errors are shown).

B: NADH coupled GTPase assay data showing the k_{obs} values corresponding to GDP turnover by MglA in the presence of RomX. MglA with MglB is shown as a positive control. The black line represents the mean and the coloured bars represent the standard error.

C: Representative plots (from n=3 repeats) showing *mant*-GMPPNP association assay of MglA with RomX. At 400 s, the protein was added, as shown by the arrow. RomX (in orange) stimulates the release of GDP on MglA and uptake of *mant*-GMPPNP in a 1:2 ratio (MglA 3 μM: RomX 6 μM), whereas MglA alone (in green) does not show exchange. The RomX mutants at the MglA interface ($RomX^{R11,14A}$ in magenta and $RomX^{D19A}$ in blue) also show abrogated nucleotide exchange activity.

D: AlphaFold model of MglA (in green) with RomX (purple) with MglA-GTP (in gray) superimposed. In the bottom inset, the interface residues are highlighted (MglA residues in green and RomX residues in purple). MglA P-loop, Switch I, and Switch II are highlighted in orange, pink, and cyan, respectively.

E: Weblogo showing the conservation of residues in RomX interfacing with MglA. The candidate residues are highlighted and their positions are labeled below.

F: ITC thermogram of a representative binding assay showing the titration of $RomX^{R11,14A}$ with MglA in the presence of GTP and magnesium. The top panel shows the raw data of heat pulses with time. The lower panel shows the corresponding heat exchange, which could not be reliably fitted to a binding curve, indicating no binding

Figure 3. RomX interacts with RomR-REC and not with RomR-Ct.

A: Schematic showing the domains of RomR, N-terminal REC domain, a long-disordered linker followed by a C-terminal helical domain.

B: The different domain-wise dissected constructs of RomR that were designed for this study. The colors of the REC and the C-terminal domains are as per A. The residue numbers of the boundaries are labeled.

C: Superdex 75 coupled with multi-angle light scattering to show the interaction of RomR-REC^{141} and RomX. The molar mass of the corresponding peaks is plotted on the right y-axis. RomX is in orange, RomR-REC^{141} is in red, and complex is in magenta. The observed and expected molar mass and the respective elution volumes are tabulated on the right.

D. ITC thermogram showing the titration of RomX with RomR-REC^{125}. The left panel shows the raw data of exothermic heat pulses with time, the middle panel shows the corresponding differential binding curve fitted to a single site binding model and the right panel shows the signature plot detailing the ΔG, ΔH and -TΔS values corresponding to the same reaction (mean and standard errors are shown).

E: Analytical Superdex 200 run showing no interaction of RomR-Ct with RomX. REC-Ct+RomX (orange), RomR-Ct (brick red), RomR + RomX (magenta).

F: AlphaFold model of RomR-Ct in complex with RomX. The low pLDDT scores are highlighted in the regions labeled in green and yellow.

Figure 4. Interface residues between RomR-REC and RomX are held by salt-bridge interaction.

A: AlphaFold model of RomR-REC (blue) and RomX complex. Experimentally obtained RomX structure in blue-gray is superposed on the model in purple. On the right, the interface of the complex is expanded showing the probable interface residues, W87 and R76 in RomX and E108 in RomR. The interacting distance between RomR E108 and RomX R76 is highlighted. The conformational change of RomX W87 across the monomeric (blue) and complex states (grey) is also shown.

B, C: Weblogos showing the conservation of residues in RomR-REC and RomX interfaces, respectively. The candidate residues are highlighted and their positions are labeled below.

D, E. Tryptophan fluorescence spectra to determine the complex formation RomR-REC and RomX in WT and mutants (left and right, respectively). RomX is titrated with increasing concentrations of RomR-REC as shown in the legend.

F, G. Relative fluorescence intensity at emission maxima λmax and the corresponding λmax values are plotted against the concentration of RomR-REC to determine the shift in fluorescence spectra as well as quenching due to complex formation, due to change in the environment of the Trp87 at the RomRX interface. The mean of 3 replicates is plotted with the error bars indicating standard errors.

H: ITC thermogram of a representative binding assay showing the titration of $RomX^{L75,R76A}$ with RomR-REC. The top panel shows the raw data of heat pulses with time. The lower panel shows the corresponding heat exchange, which could not be reliably fitted to a binding curve, indicating no binding.

Figure 5. RomX is sandwiched between MglA and RomR-REC.

A: AlphaFold model of MglA (in green), RomR (in dark blue) and RomX (in purple) predicts RomX sandwiched between MglA and RomX. MglA model is superposed with MglA-GTP (PDB ID: 6IZW, in gray).

B: NADH coupled GTPase assay data showing that none of the RomR constructs with or without RomX shows GAP activity as observed with MglB. The black line represents the mean and the coloured bars represent the standard error.

C and D: Representative plots showing *mant*-GMPPNP association assays of MglA with RomR REC^{125}, and RomR-Ct domains, respectively. The trend was similar for both cases. RomX (orange) stimulates the release of GDP on MglA and uptake of *mant*-GMPPNP in a 1:2

ratio and the rates are similar with RomX+ RomR (blue) in the same 1:2 ratio (MglA 3 μM : RomRX 6 μM), whereas RomR alone (brick red) does not stimulate exchange. n=3 repeats performed for each MglA, MglA+RomX, MglA+RomR-REC^{125}, MglA+RomR-REC^{125}+RomX, MglA+RomR-Ct, MglA+RomR-Ct+RomX, runs.

Figure 6. RomX maintains *M. xanthus* cell polarity by regulating MglA localization.

A: Mechanism of stimulation of nucleotide exchange on MglA by RomX. RomX preferentially binds and sequesters MglA-GTP facilitating nucleotide exchange.

B: Model showing the mechanism of polarity maintenance in *M. xanthus*. At the lagging pole RomX (in purple) generates local pools of MglA-GTP, ready to be hydrolyzed by MglB-RomY, thereby excluding MglA. At the leading pole, RomX recruits MglA-GTP which is probably facilitated by interaction with additional effectors (in teal).

Figure 1

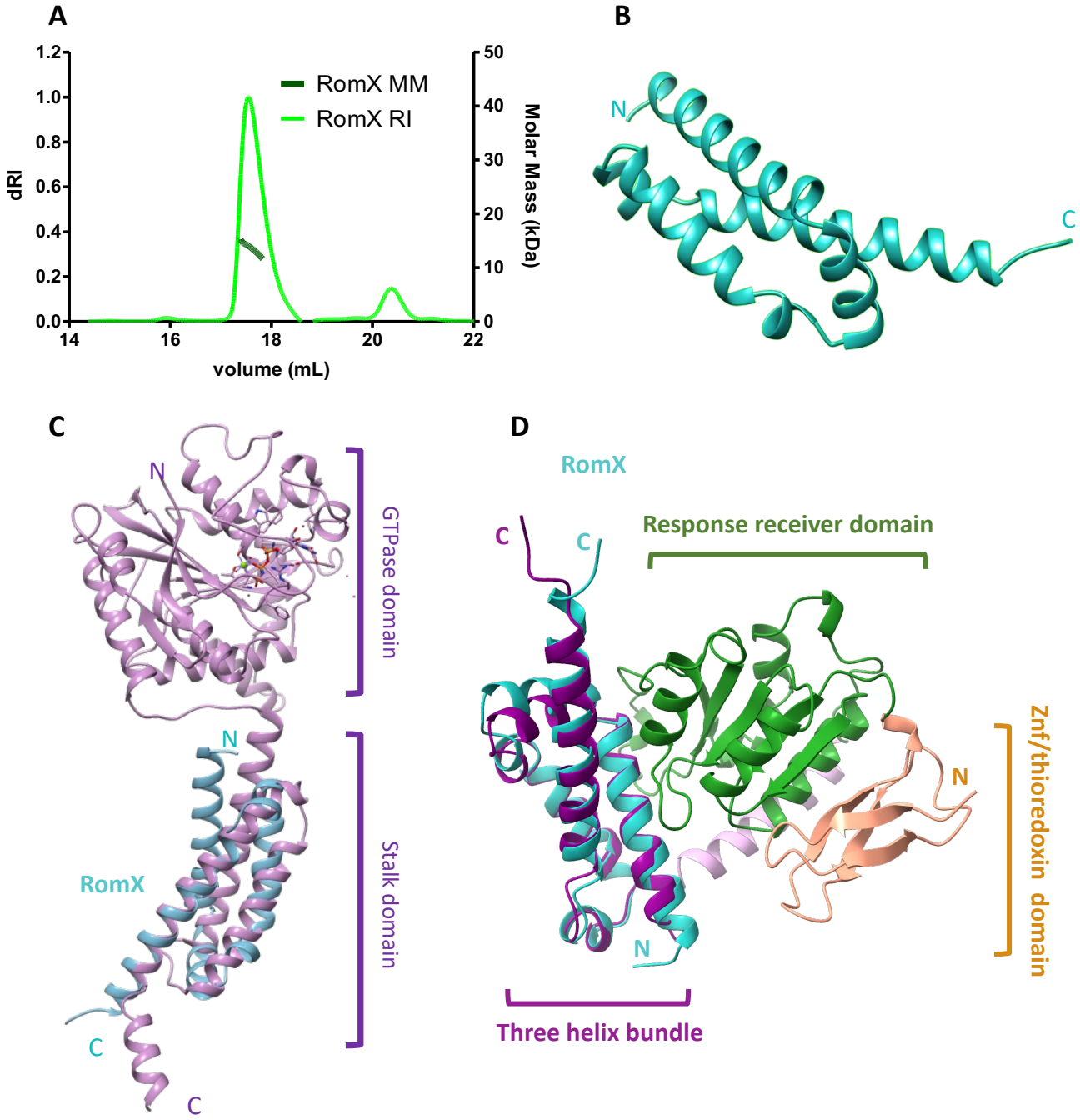
A
RomX MM
RomX RI
dRI
Molar Mass (kDa)
volume (mL)
B
N
C
C
GTPase domain
N
N
Stalk domain
RomX
C
C
D
RomX
C
C
Response receiver domain
N
N
Znf/thioredoxin domain
Three helix bundle

Figure 2

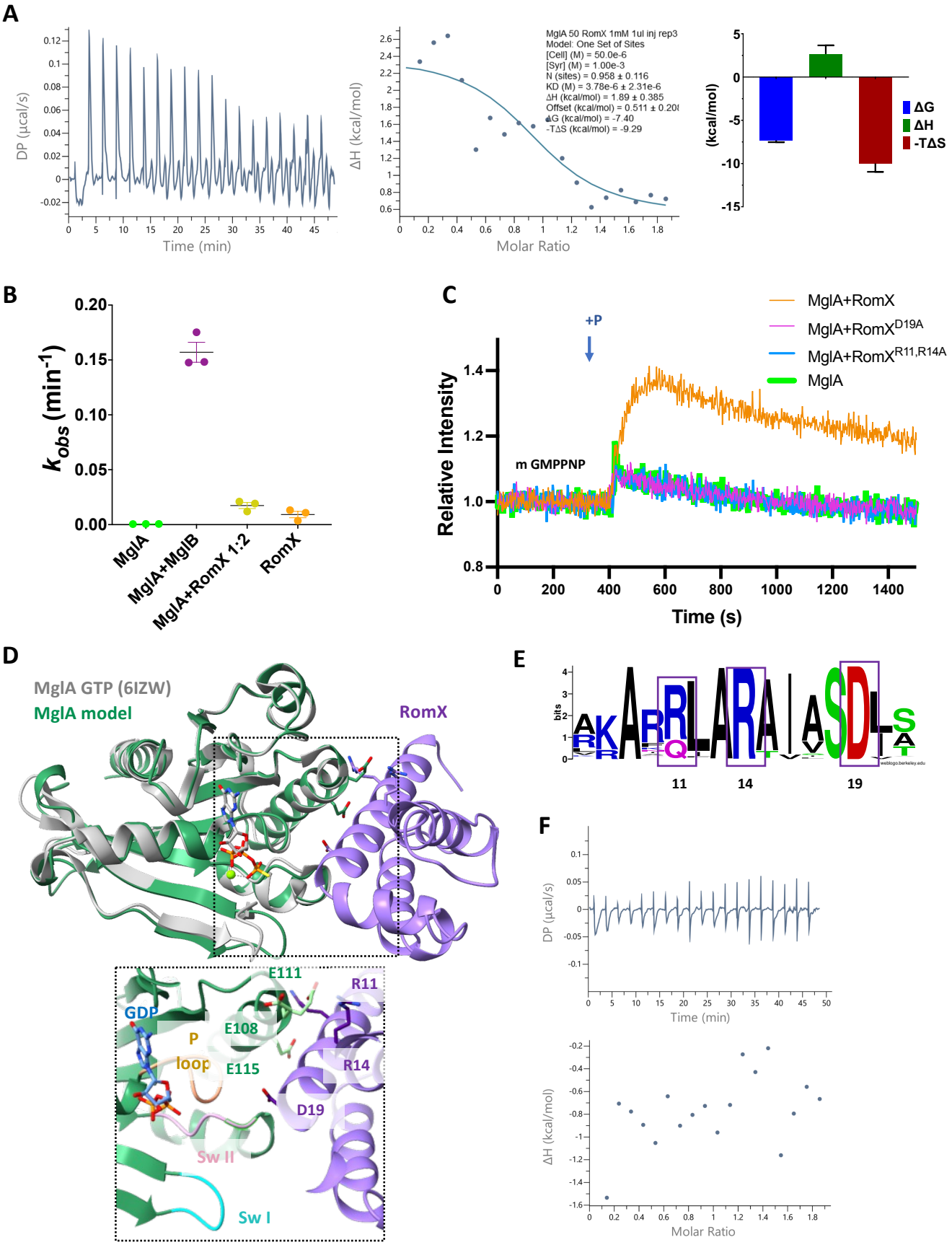
A
DP (µcal/s)
Time (min)
ΔH (kcal/mol)
Molar Ratio
MglA 50 RomX 1mM 1ul inj rep3
Model: One Set of Sites
[Cell] (M) = 50.0e-6
[Syr] (M) = 1.00e-3
N (sites) = 0.958 ± 0.116
KD (M) = 3.78e-6 ± 2.31e-6
ΔH (kcal/mol) = 1.89 ± 0.385
Offset (kcal/mol) = 0.511 ± 0.20
ΔG (kcal/mol) = -7.40
-TΔS (kcal/mol) = -9.29
(kcal/mol)
ΔG
ΔH
-TΔS
B
k_{obs} (min^{-1})
MglA
MglA+MglB
MglA+RomX 1:2
RomX
C
+P
m GMPPNP
Relative Intensity
Time (s)
MglA+RomX
MglA+RomX^{D19A}
MglA+RomX^{R11,R14A}
MglA
D
MglA GTP (6IZW)
MglA model
RomX
E111
R11
GDP
E108
P
loop
E115
R14
D19
Sw II
Sw I
E
bits
11
14
19
F
DP (µcal/s)
Time (min)
ΔH (kcal/mol)
Molar Ratio

Figure 3

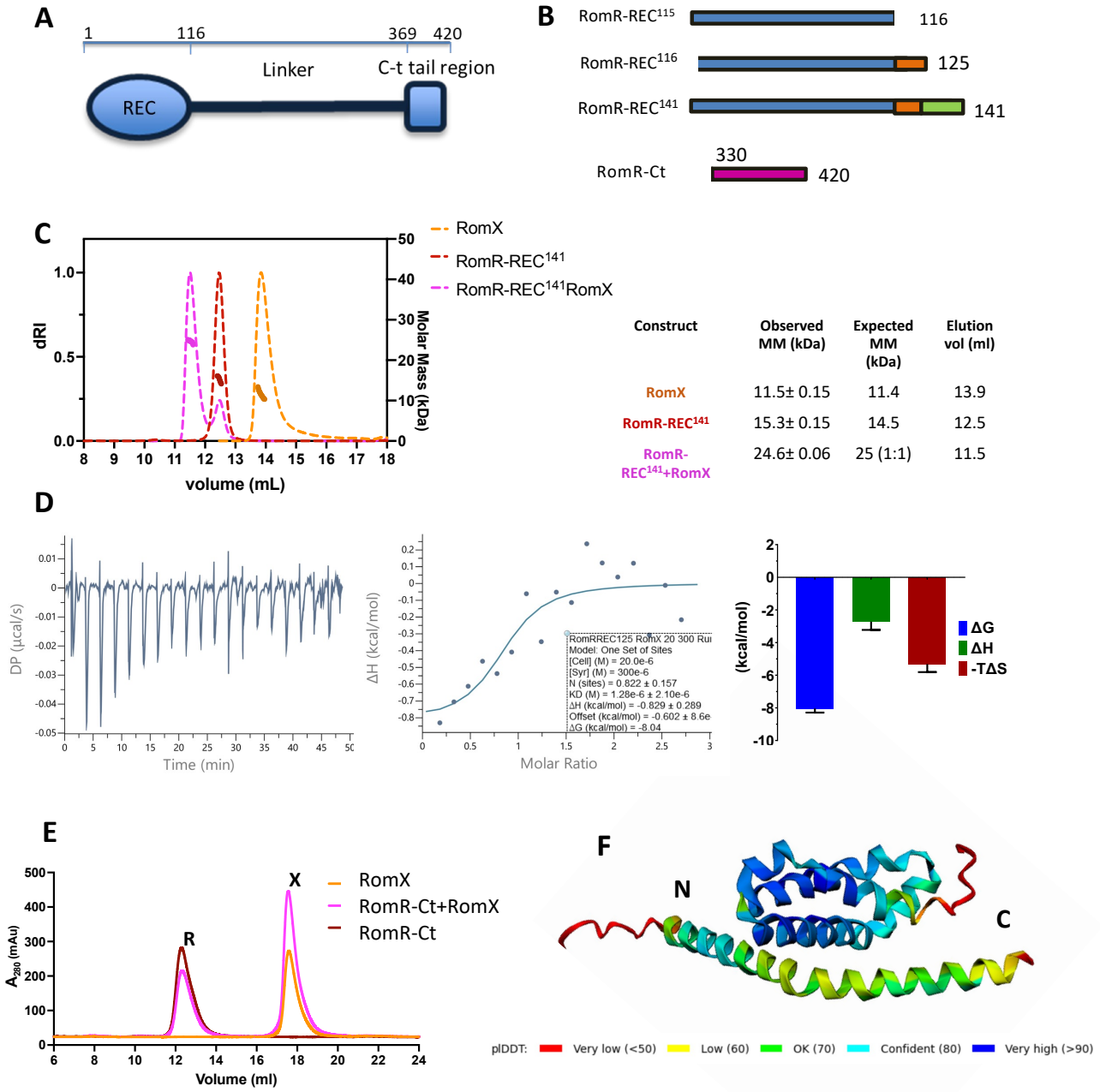

Construct	Observed MM (kDa)	Expected MM (kDa)	Elution vol (ml)
RomX	11.5± 0.15	11.4	13.9
RomR-REC141	15.3± 0.15	14.5	12.5
RomR-REC141+RomX	24.6± 0.06	25 (1:1)	11.5

Figure 4

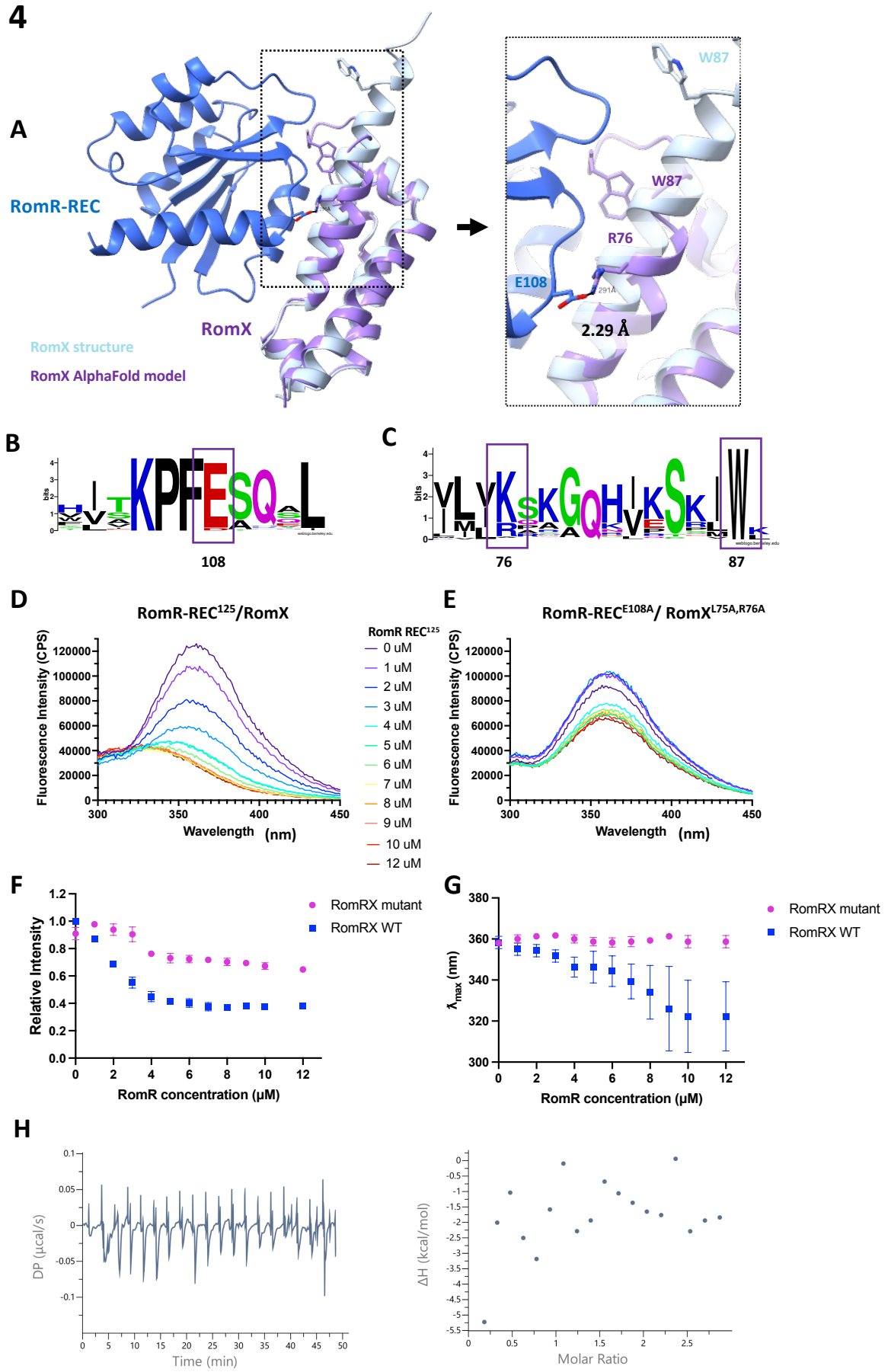
A
RomR-REC
RomX
RomX structure
RomX AlphaFold model
W87
W87
R76
E108
2.29 Å
B
108
C
76
87
D
RomR-REC125/RomX
Fluorescence Intensity (CPS)
Wavelength (nm)
RomR REC125
0 uM
1 uM
2 uM
3 uM
4 uM
5 uM
6 uM
7 uM
8 uM
9 uM
10 uM
12 uM
E
RomR-RECE108A/ RomXL75A,R76A
Fluorescence Intensity (CPS)
Wavelength (nm)
F
Relative Intensity
RomR concentration (μM)
RomRX mutant
RomRX WT
G
λmax (nm)
RomR concentration (μM)
RomRX mutant
RomRX WT
H
DP (μcal/s)
Time (min)
ΔH (kcal/mol)
Molar Ratio

Figure 5

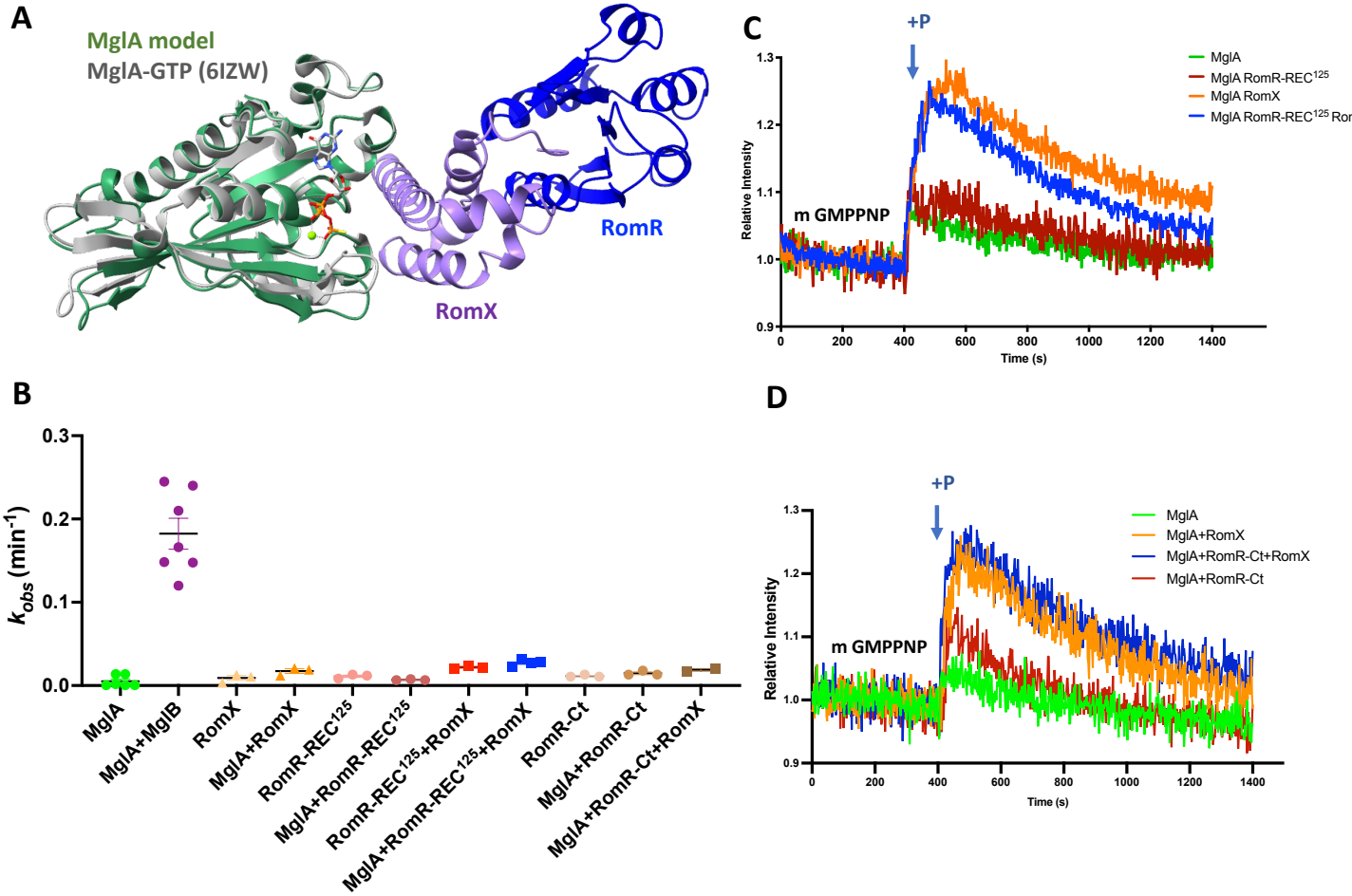
A
MglA model
MglA-GTP (6IZW)
RomR
RomX
B
k_{obs} (min^{-1})
0.3
0.2
0.1
0.0
MglA
MglA+MglB
RomX
MglA+RomX
RomR-REC^{125}
MglA+RomR-REC^{125}
RomR-REC^{125}+RomX
MglA+RomR-REC^{125}+RomX
RomR-Ct
MglA+RomR-Ct
MglA+RomR-Ct+RomX
C
+P
m GMPPNP
Relative Intensity
Time (s)
MglA
MglA RomR-REC^{125}
MglA RomX
MglA RomR-REC^{125} Ror
D
+P
m GMPPNP
Relative Intensity
Time (s)
MglA
MglA+RomX
MglA+RomR-Ct+RomX
MglA+RomR-Ct

Figure 6

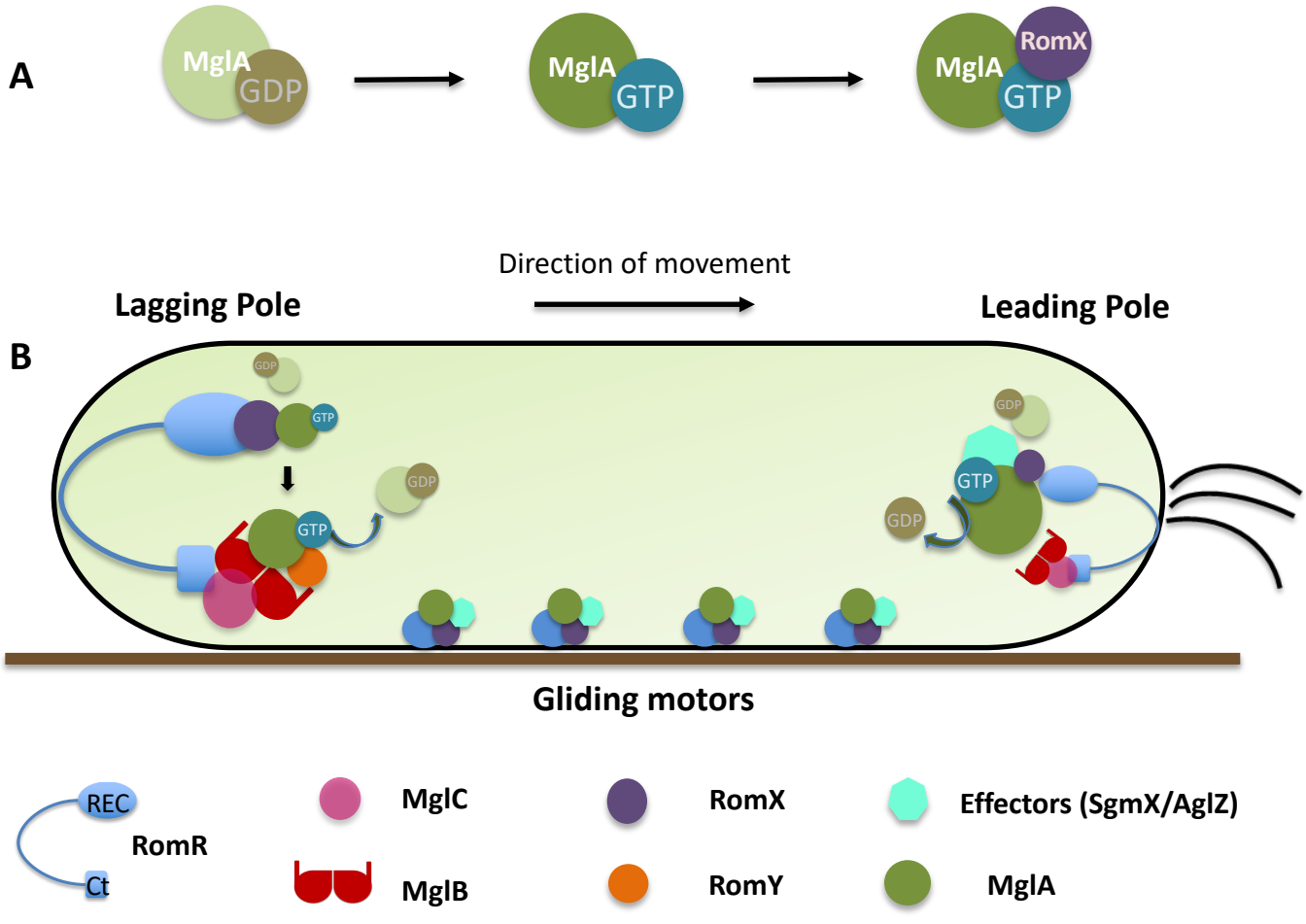
A
MglA
GDP
MglA
GTP
MglA
RomX
GTP
B
Direction of movement
Lagging Pole
Leading Pole
GDP
GTP
GDP
GTP
GDP
GTP
GDP
Gliding motors
REC
RomR
Ct
MglC
MglB
RomX
RomY
Effectors (SgmX/AglZ)
MglA